Journal of Genetics and Genomics 50 (2023) 253–263

Contents lists available at ScienceDirect

Journal of Genetics and Genomics

Journal homepage: www.journals.elsevier.com/journal-of-genetics-and-genomics/

Original research

Ccdc57 is required for straightening the body axis by regulating ciliary motility in the brain ventricle of zebrafish

Lu Li [a, b, 1], Juan Li [a, b, 1], Yuan Ou [a, b], Jiaxin Wu [c], Huilin Li [a, b], Xin Wang [a, b], Liying Tang [b], Xiangyan Dai [d], Conghui Yang [a, b], Zehong Wei [a, b], Zhan Yin [e], Yuqin Shu [a, b, *]

[a] State Key Laboratory of Developmental Biology of Freshwater Fish, College of Life Sciences, Hunan Normal University, Changsha, Hunan 410081, China
[b] College of Life Sciences, Hunan Normal University, Changsha, Hunan 410081, China
[c] School of Life Sciences, East China Normal University, Shanghai 200241, China
[d] Key Laboratory of Freshwater Fish Reproduction and Development, Ministry of Education, Southwest University, Chongqing 400715, China
[e] State Key Laboratory of Freshwater Ecology and Biotechnology, Institute of Hydrobiology, Chinese Academy of Sciences, Wuhan, Hubei 430072, China

ARTICLE INFO

Article history:
Received 19 July 2022
Received in revised form
22 December 2022
Accepted 31 December 2022
Available online 18 January 2023

Keywords:
Scoliosis
CSF
ccdc57
Cilia
Epinephrine
Urotensin

ABSTRACT

Recently, cilia defects have been proposed to contribute to scoliosis. Here, we demonstrate that coiled-coil domain-containing 57 (Ccdc57) plays an essential role in straightening the body axis of zebrafish by regulating ciliary beating in the brain ventricle (BV). Zygotic *ccdc57* (*Zccdc57*) mutant zebrafish developes scoliosis without significant changes in their bone density and calcification, and the maternal-zygotic *ccdc57* (MZ*ccdc57*) mutant embryos display curved bodies since the long-pec stage. The expression of *ccdc57* is enriched in ciliated tissues and immunofluorescence analysis reveals colocalization of Ccdc57-HA with acetylated α-tubulin, implicating it in having a role in ciliary function. Further examination reveals that it is the coordinated cilia beating of multiple cilia bundles (MCB) in the MZ*ccdc57* mutant embryos that is affected at 48 hours post fertilization, when the compromised cerebrospinal fluid flow and curved body axis have already occurred. Either *ccdc57* mRNA injection or epinephrine treatment reverses the spinal curvature in MZ*ccdc57* mutant larvae from ventrally curly to straight or even dorsally curly and significantly upregulates urotensin signaling. This study reveals the role of *ccdc57* in maintaining coordinated cilia beating of MCB in the BV.

Introduction

Coiled-coil domain-containing (CCDC) proteins essentially contain the highly conserved coiled-coil domain, a superhelical protein motif consisting of one or more alpha-helical peptides wrapped around each other (Burkhard et al., 2001). The canonical coiled-coil is characterized by a heptad repeat of seven-residue periodicity, and the hydrophobic amino acids at positions a and d are conserved. The noncanonical motifs are also formed from repeating hydrophobic residues spaced apart by insertions of extra amino acids (1, 2, 3, 4, or 6). Usually, the insertions result in discontinuities in the heptad repeat and local structural deformations in the coiled coil. Alpha-helices of the same chain or different chains may form homo- or hetero-oligomers in parallel or antiparallel orientations (Lupas, 1996; Harbury et al., 1998; Stetefeld et al., 2000; Truebestein and Leonard, 2016; Lupas et al., 2017).

CCDC proteins are widely expressed in nearly all kinds of tissues and function in most physiological processes, including ciliogenesis (Rose et al., 2005; Rackham et al., 2010; Priyanka and Yenugu, 2021). Cilia are evolutionarily conserved structures, and their axoneme consists of nine doublet microtubules with or without a pair of single microtubules in the center (Malicki et al., 2011; Ishikawa, 2017). They play key roles in diverse cell types, and defects in motile cilia cause the most prominent ciliopathy known as primary ciliary dyskinesia (PCD). The clinical manifestations of PCD patients include pulmonary disease, chronic or recurrent ear infection, infertility, situs inversus and heterotaxy (Escudier et al., 2009).

A series of mutations in CCDC proteins have been identified as the cause of PCD with iron deficiency anemia (IDA) defects and axonemal disorganization, and these patients develop infertility, situs

* Corresponding author.
E-mail address: shuyuqin@hunnu.edu.cn (Y. Shu).
[1] These authors contributed equally to this work.

https://doi.org/10.1016/j.jgg.2022.12.007

inversus and heterotaxy (Mahjoub et al., 2010; Becker-Heck et al., 2011; Blanchon et al., 2012; Horani et al., 2013; Knowles et al., 2013a; Onoufriadis et al., 2013; Wu and Singaraja, 2013; Hjeij et al., 2014; Sui et al., 2016; Li et al., 2019; Cannarella et al., 2020; Chen et al., 2020, 2021; Deng et al., 2020; Ochi et al., 2020; Pizon et al., 2020). There are more than 28 mutations of CCDC39 and CCDC40 reported so far, representing the major cause of PCD (Becker-Heck et al., 2011; Blanchon et al., 2012; Sui et al., 2016; Cannarella et al., 2020; Chen et al., 2021).

Among these CCDC proteins, eight members (CCDC39, CCDC40, CCDC65, CCDC104, CCDC114, and CCDC151) colocalize with the axoneme of cilia. CCDC39 and CCDC40 are required for the assembly of the inner dynein arm and the dynein regulatory complex. The absence of either CCDC39 or CCDC40 causes axonemal disorganization and abnormal ciliary beating (Becker-Heck et al., 2011; Merveille et al., 2011). CCDC65 forms the "base plate" of the nexin-dynein regulatory complex (N-DRC), which makes extensive connections with the outer doublet microtubules, radial spokes, and inner dynein arms (Austin-Tse et al., 2013; Horani et al., 2013). CCDC96 and CCDC113 are positioned parallel to N-DRC and form a connection between radial spoke 3, dynein g, and N-DRC (Bazan et al., 2021). CCDC104 is an ARL3-interacting protein and is enriched at the base of the cilium (Lokaj et al., 2015). CCDC114 is an ODA microtubule-docking complex component and is required for microtubular attachment of ODAs to the axoneme (Onoufriadis et al., 2013). CCDC151 plays important roles in the control of intraflagellar transport (IFT)-dependent dynein arm assembly (Jerber et al., 2014).

In addition, another seven members (CCDC11, CCDC41, CCDC61, CCDC68, CCDC120, CCDC113, and CCDC57) were identified as centrosome-associated proteins. Centrosomes function as basal bodies for cilia formation and are essential for nucleating the axoneme (Joo et al., 2013; Silva et al., 2016; Huang et al., 2017; Gurkaslar et al., 2020; Pizon et al., 2020; Bazan et al., 2021). CCDC11, CCDC57, and CCDC113 are components of centriolar satellites and are required for ciliogenesis (Firat-Karalar et al., 2014; Silva et al., 2016). CCDC41 specifically localizes to the distal end of the mother centriole and recruits IFT protein 20 to the centrosome (Joo et al., 2013). CCDC61, CCDC68, and CCDC120 have been identified as subdistal appendage components and are required for centrosome microtubule anchoring (Huang et al., 2017; Pizon et al., 2020). Knockdown of CCDC57 and CCDC61 causes a delay in cilia formation in RPE-1 cells, which suggests they have a role in promoting ciliogenesis (Gurkaslar et al., 2020; Ochi et al., 2020).

CCDC57 is minimally characterized and is associated with bovine milk fat composition and uterine leiomyomata in several studies using genome-wide research (Bouwman et al., 2014; Aissani et al., 2015; Alleyne and Bideau, 2019; Bohlouli et al., 2022). The function of CCDC57 has been investigated only in mammalian cell lines. CCDC57 localizes to the centrosome and microtubules through distinct domains and is required for centriole duplication through the recruitment of centrosomal protein 63 (CEP63) and CEP152. The absence of CCDC57 causes defects in cilium assembly, centriolar satellite distribution, mitotic progression, and microtubule nucleation (Gurkaslar et al., 2020). However, the function of CCDC57 in vivo remains unclear.

Zebrafish is an ideal model to investigate ciliary function due to their transparent embryos. Based on zebrafish models, cilia defects have been reported to cause scoliosis in *protein-tyrosine kinase-7* (*ptk7*) mutant patients and zebrafish (Hayes et al., 2014). The *ptk7* mutant zebrafish develops scoliosis and exhibits defective cilia development and cerebrospinal fluid (CSF) flow. In addition, the spinal curve progression of *c21orf59*^{TS} mutant zebrafish could be blocked by the restoration of cilia motility (Grimes et al., 2016). Other studies suggested that adrenergic signals transported by CSF flow are essential to straighten the body axis by activating urotensin signaling and promoting fiber contraction on the dorsal smite (Zhang et al., 2018).

In this study, we established a *ccdc57* knockout zebrafish model to characterize the function of Ccdc57 in vivo. It was found that *ccdc57* deficiency resulted in scoliosis in zebrafish. The distribution of *ccdc57* mRNA was restricted to ciliated organs, such as the brain ventricle (BV), otic vesicles, and inner nuclear layer, during the embryonic stage and was especially enriched in the BV, which is filled with cilia attached to ependymal cells around the surface to drive CSF flow. Then, Ccdc57-HA was found to associate with acetylated α-tubulin on the axoneme of cilia. Maternal depletion of *ccdc57* caused a curved body axis accompanied by an abnormal cilia beat pattern and compromised CSF flow. The defective CSF flow could further lead to hydrocephalus and cilia defects. Additionally, treatment with epinephrine or injection with wild-type (WT) *ccdc57* mRNA could revise the curved body axis into straight and even dorsally curly and upregulated urotensin signaling. Taken together, our study strongly demonstrates that Ccdc57 plays an essential role in straightening the body axis by regulating ciliary motility in the BV of zebrafish.

Results

Depletion of *ccdc57* causes scoliosis in zebrafish

ccdc57-depleted zebrafish were generated using the CRISPR/Cas9 targeting technique. The 20 bp target sequences were designed against the first exon of *ccdc57* based on the sequence information got from NCBI. Two independent mutant lines were obtained with 10- or 4-base pair deletions in the target region of *ccdc57* (Fig. 1A). The WT-*ccdc57* mRNA is translated into a protein with 979 amino acids, while the mutant Ccdc57 retains only 92 and 94 amino acids due to early termination of translation, containing 63 and 65 correct amino acids, respectively (Fig. S1).

Raised under the same conditions, the WT and *ccdc57* mutant zebrafish consisted of both female and male individuals without obvious growth differences. In contrast to WT zebrafish with a straight body axis, all *ccdc57* mutants displayed scoliosis, characterized by three-dimensional spinal curvature at three months post fertilization (mpf) (Fig. 1B). At the protruding-mouth stage, the end of the spine became ventrally curly in most maternal-zygotic *ccdc57* (MZ*ccdc57*) mutants, but the WT embryos displayed a straight body axis at the same stage. When raised up to 20 days post fertilization (dpf), the curved spine developed into scoliosis in MZ*ccdc57* mutants, but the WT larvae maintained a straight body axis (Fig. 1C). The rate of spinal curvature was extremely low in WT embryos and became zero in WT adults. However, the rate reached nearly eighty percent in MZ*ccdc57* mutant embryos and reached one hundred percent in MZ*ccdc57* mutant adults (Fig. 1D).

High-resolution microscale computed tomography (micro-CT) was performed to examine the vertebral bone density and structure in Zygotic *ccdc57 (Zccdc57)*-depleted zebrafish. Six replicates of WT and Z*ccdc57* mutant zebrafish assayed by micro-CT revealed different types of three-dimensional spinal malformations in *ccdc57*-depleted zebrafish. Except for the curvature, the spines of the mutants were rather normal without deletion or fracture of the vertebrae. Based on the direction of curvature, the *ccdc57*-depleted zebrafish were classified into three types (Fig. 2A), and the three types accounted for 22%, 51%, and 27% respectively (Fig. S2). The vertebral bone densities of WT and *ccdc57*-depleted zebrafish were also assayed by micro-CT, which revealed no significant differences between them (Fig. 2B). The bone formation of WT and MZ*ccdc57*-depleted zebrafish was examined using calcein staining at 11 dpf and 14 dpf, respectively, when some of the

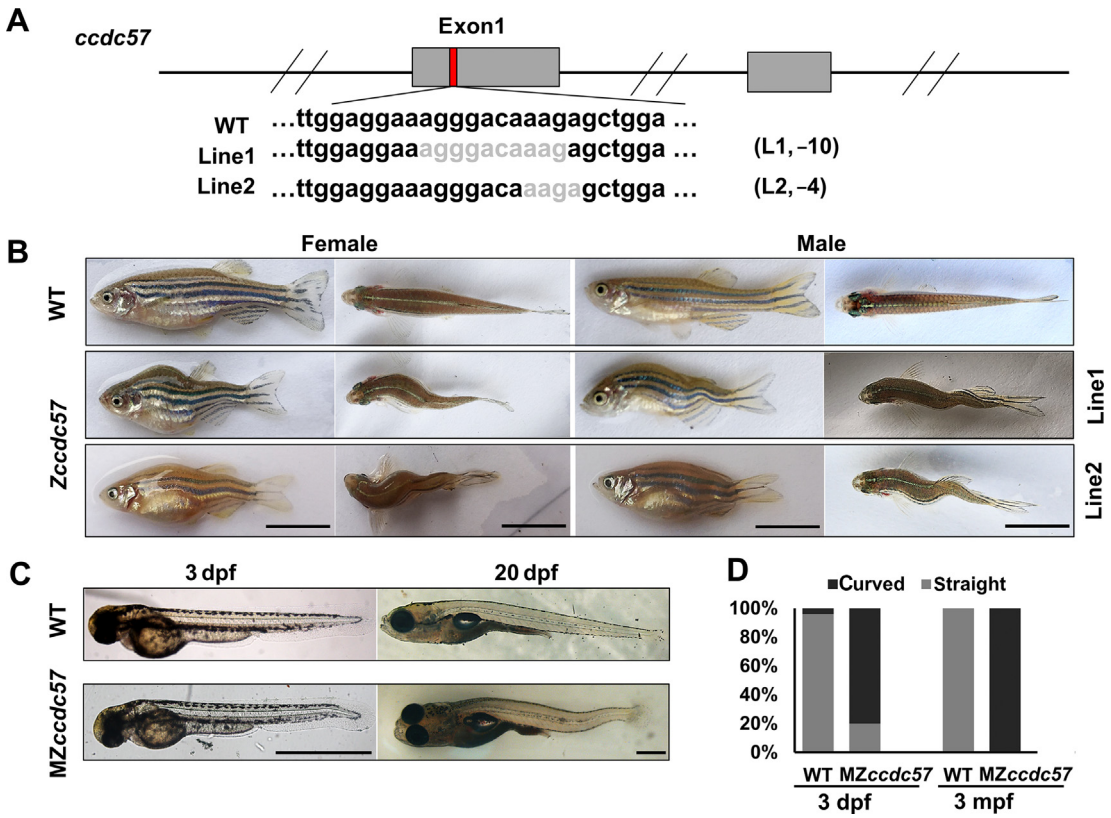

Fig. 1. Depletion of *ccdc57* results in scoliosis in zebrafish. **A**: The target in the first exon of *ccdc57* and two mutant lines with 10- and 4-bp deletions were established. **B**: Representative body axis of wild type (WT) and *ccdc57* mutant zebrafish at 3 mpf. Both female and male WT zebrafish exhibited straight body axes in lateral and dorsal views. Female and male zebrafish of the two mutant lines exhibited scoliosis in lateral and dorsal views. **C**: Representative body axis of WT and MZ*ccdc57* mutant zebrafish at early stages. WT larvae and juveniles exhibited straight body axes at 3 dpf and 20 dpf. The MZ*ccdc57* mutant larvae showed ventral curvature at the end of the tail at 3 dpf, and the mutant juveniles developed scoliosis at 20 dpf. **D**: Statistical analysis of the rates of curvature or scoliosis at 3 dpf and 3 mpf. Scale bars, 1 cm (**B**); 1 mm (**C**). dpf, days post fertilization; mpf, months post fertilization.

MZ*ccdc57* mutants displayed scoliosis, and the results suggested that they shared the same vertebral patterning (Fig. 2C).

Ccdc57 localizes to microtubules

To explore the in vivo role of *ccdc57*, its expression pattern during embryonic development was examined. As shown by RT-PCR analysis, *ccdc57* was expressed throughout embryogenesis (Fig. S3A). qPCR analysis identified higher *ccdc57* expression at 12 h and 24 h than in the other stages examined (Fig. S3B). Whole-mount in situ hybridization analysis was carried out to characterize the spatial expression of *ccdc57* at the one-cell, two-cell, high, 6-somite, prim-5, long-pec, and protruding mouth stages. The expression of *ccdc57* was ubiquitous from the one-cell to 6-somite stage (Fig. S3C–S3F). At the prim-5 stage, the expression of *ccdc57* was restricted to the BV, otic vesicle, and inner nuclear layer, and was especially higher in the hind BV (Fig. 3A). At the long-pec stage, *ccdc57* mRNA was mainly located in the BV, otic vesicle, and branchial primordium (Fig. S3G and S3H). These *ccdc57*-expressing regions, including the BV, otic vesicle, and inner nuclear layer, are known as cilia-enriched tissue. At the adult stage, *ccdc57* mRNA was enriched in ciliary organs, including the eye, brain, kidney, testis, and ovary (Fig. 3B).

Due to the absence of a working antibody, an HA-tag was added to the C-terminal end of Ccdc57 to investigate its subcellular localization. The *HA*-tagged *ccdc57* mRNA was transcribed and injected into one-cell stage embryos at a concentration of 15 ng/μL. Then, the injected embryos were fixed, and whole-mount immunofluorescence was carried out with a mouse anti-acetylated α-tubulin antibody and a rabbit anti-HA antibody to label the cilia axoneme. Surprisingly, in both BV and otic vesicles, HA-Ccdc57 was associated with acetylated α-tubulin on the axoneme (Fig. 3C–3H). In order to avoid the cross-reactivity of the anti-acetylated α-tubulin antibody with the anti-HA antibody, the whole-mount immunofluorescence was also carried out individually with the anti-acetylated α-tubulin antibody or the anti-HA antibody and the results showed similar signals (Fig. S3I and S3J). These results suggested a ciliary role of *ccdc57* in zebrafish.

Ccdc57 deficiency leads to BV cilia defects and hydrocephalus in adult zebrafish

To explore the ciliary role of Ccdc57, ciliogenesis in BV was examined by immunofluorescence. The cilia in BV were much shorter than cilia in the spinal canal at 48 hpf, but no obvious differences in lengths and morphology were found between WT and MZ*ccdc57* mutant embryos (Fig. 4A). Furthermore, the analysis of cilia densities revealed no significant differences (Fig. 4B). Cilia ciliogenesis was not affected in MZ*ccdc57* mutant embryos at 48 hpf when the curved body axis had occurred. It is easy to speculate that ciliary motility defects may be responsible for the curvature of the spine. However, examination of cilia in adult BV by scanning electron microscopy suggested severe cilia defects in *ccdc57* mutant zebrafish. The cilia in these mutants were sparse, curly, and disorderly, while those in WT zebrafish were dense, organized, and polarized (Fig. 4C–4H). The cilia density in *ccdc57* mutant zebrafish was significantly lower than in WT zebrafish (Fig. 4I). In addition, the

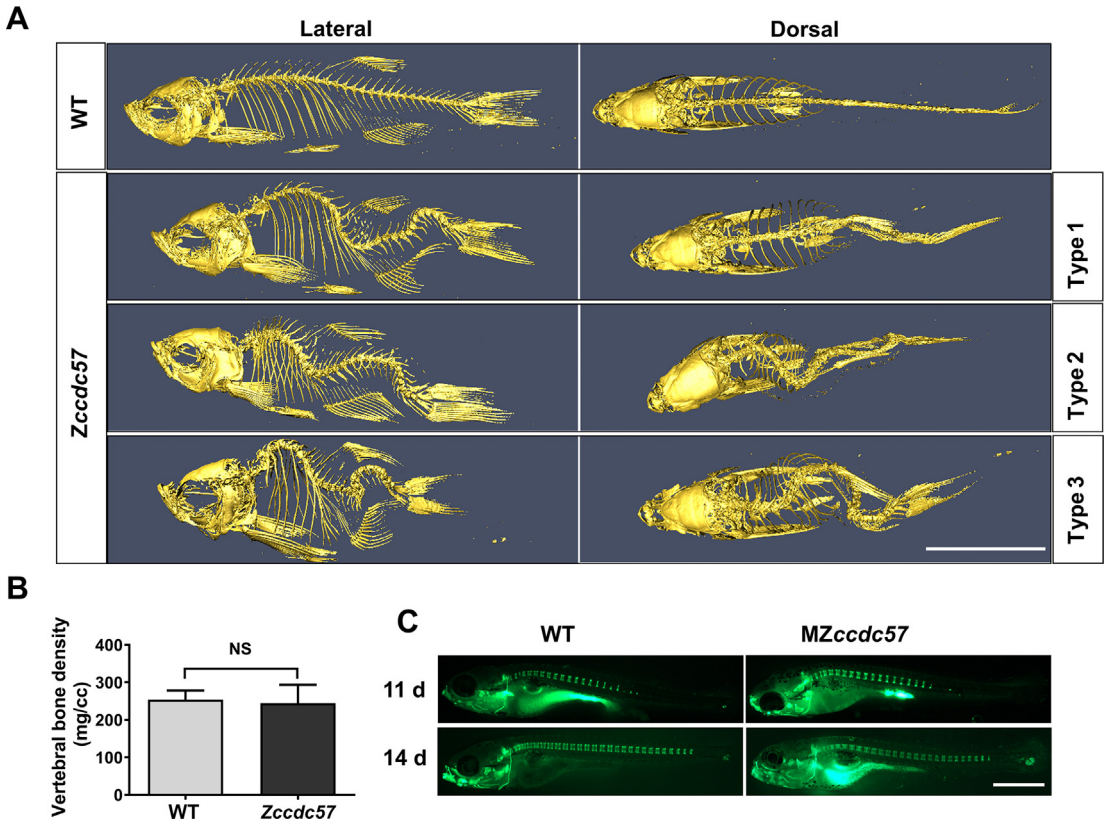

Fig. 2. *ccdc57* mutants develop three-dimensional spinal curvature without defects in calcification and bone density. **A**: Three-dimensional image of the skeletal system reconstructed from micro-CT scans of adult WT and *Zccdc57* mutant zebrafish from lateral and dorsal views. Type 1 represents scoliosis in the vertical dimension. Type 2 represents scoliosis curving leftward to rightward in the horizontal dimension. Type 3 represents scoliosis curving rightward to leftward. **B**: No significant difference in vertebral bone densities between WT and *Zccdc57* mutant zebrafish assayed by micro-CT. **C**: Live calcein staining of WT zebrafish and MZ*ccdc57* mutants at 11 dpf and 14 dpf. Data were presented as mean ± SD. Statistical analysis was performed by Student's *t*-test. NS, no significant difference. Different types in (**A**) indicate different shapes of curvature. Scale bars, 1 cm (**A**); 1 mm (**C**). micro-CT, microscale computed tomography; dpf, days post fertilization; SD, standard error.

ccdc57 mutant zebrafish also displayed severe hydrocephalus characterized by an enlarged BV (Fig. 4J and 4K), a typical phenotype associated with cilia dysfunction.

Ccdc57 deficiency results in abnormal ciliary beat patterns and compromised CSF flow

Since Ccdc57 is not required for ciliogenesis, hydrocephalus could be resulted from defects in ciliary motility. Thus, the CSF flow was assayed by tracking the movement of fluorescent dye along the spinal canal of the embryos. The distance that dextran conjugated to rhodamine moved was imaged at 5 min, 10 min, 20 min, and 30 min after injection. The images revealed that the movement of dextran dye was compromised in *ccdc57* mutant embryos (Fig. 5A). Statistical analysis suggested that the dextran dye in WT embryos moved significantly farther than in *ccdc57* mutant embryos at 30 min (Fig. 5B).

To observe the cilia motility vividly, the cilia were labeled with RFP by injecting *arl13b-RFP* mRNA into one-cell stage embryos, and ciliary beating in BV was observed and recorded using a dragonfly microscope. It was found that the ciliary beat frequency was increased in MZ*ccdc57* mutant embryos (Fig. S4A), and the rhythmic beating of multiple cilia bundles (MCB) on ependymal cells was disrupted in MZ*ccdc57* mutants. The MCB of the WT zebrafish beat in phase (Fig. 5C; Movie S1), but the beating of MCB was out of sync in MZ*ccdc57* mutant zebrafish (Fig. 5D; Movie S2). The *ccdc57* mRNA-injected embryos of both WT and MZ*ccdc57* mutant zebrafish displayed coordinated ciliary beating (Fig. 5E and 5F; Movies S3 and S4). These results suggested that *ccdc57* was required for the coordinated beating of MCB.

Because flagellar has the same structure and function as motile cilia and *ccdc57* mRNA was enriched in the testis of zebrafish, sperm motility was also examined and analyzed by computer-assisted sperm analysis (CASA). The motile sperm of WT males displayed forward directional movement, and the trajectories were smooth, long, and nearly straight; however, the moving paths of most *ccdc57* mutant sperm were kinked and circular (Fig. 5G and 5H). The CASA also provided sperm motility parameters. The ratio of the straight-line velocity (VSL) and the curvilinear velocity (VCL) reflected the curvature of the sperm trajectory. The statistical analysis indicated that the sperm VSL/VCL was significantly lower in *ccdc57* mutant males, but the flagellum beat frequency was not affected (Figs. 5I and S4B). Further examination of the flagellar ultrastructure revealed no detectable changes in MZ*ccdc57* mutant zebrafish (Fig. S4C and S4D). These results demonstrated that *ccdc57* was required for the normal cilia beat pattern.

ccdc57 regulates the body axis through urotensin signaling in zebrafish

To determine whether the curved body axis of MZ*ccdc57* mutant larvae resulted from Ccdc57 deficiency, mRNA transcribed from WT *ccdc57* CDS was injected into both WT and *ccdc57* mutant embryos at the one-cell stage, and their body axis was imaged at 48 hpf. In contrast to the MZ*ccdc57* mutant, parts of the injected WT and *ccdc57* mutant embryos developed dorsal curvature (Fig. 6A). This

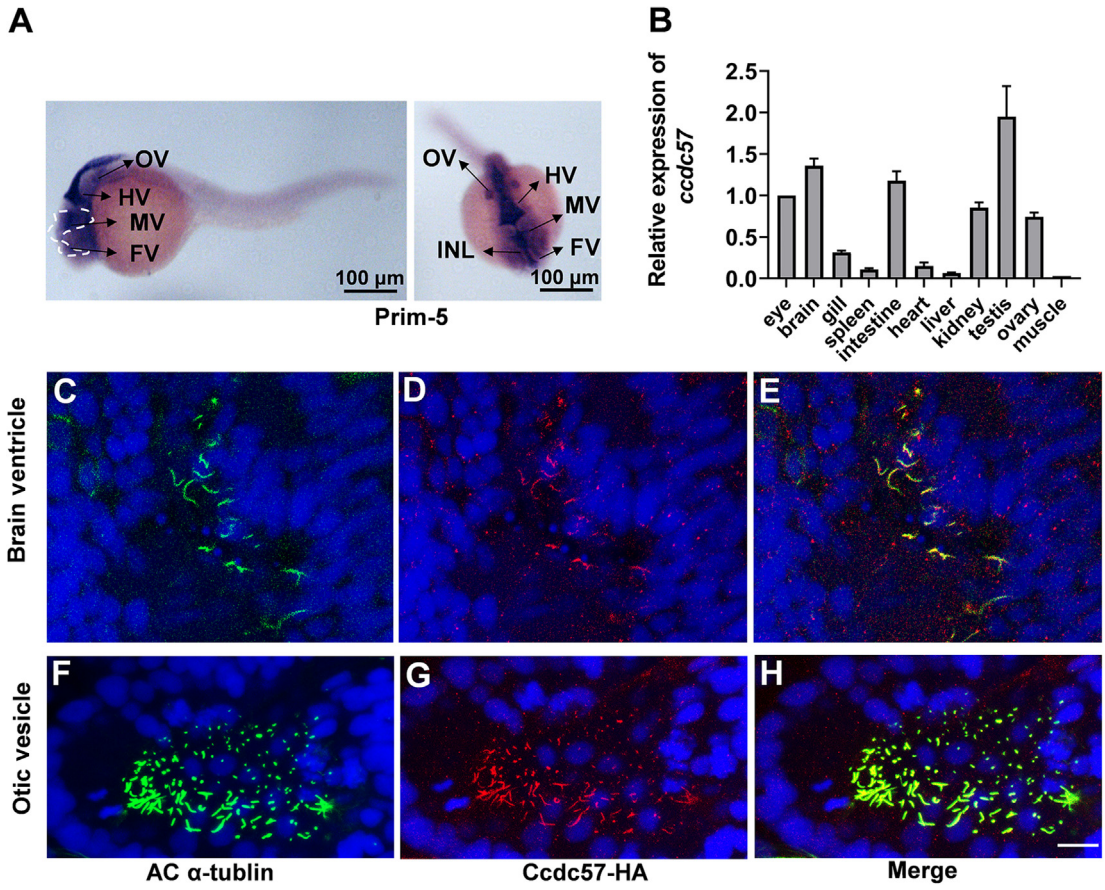

Fig. 3. Spatial expression and subcellular localization of Ccdc57 in zebrafish. **A**: *ccdc57* expression, detected by whole mount in situ hybridization, was restricted to FBV, MBV, HBV, OV, and INL in zebrafish embryos at 24 hpf. **B**: Relative expression of *ccdc57* in different tissues of adult zebrafish. Data were presented as mean ± SD. **C**–**H**: Ccdc57 is localized to ciliary axonemes in BVs and otic vesicles. The axoneme was labeled with acetylated α-tubulin antibody (green). The localization of Cccd57-HA was visualized by staining with an antibody against the HA tag (red). Nuclei were stained with DAPI (blue). Scale bars, 100 μm (**A**); 10 μm (**C**–**H**). FV, forebrain ventricle; MV, midbrain ventricle; HV, hindbrain ventricle; INL, inner nuclear layer; OV, otic vesicle; hpf, hours post fertilization.

was regarded as a result of the overexpression of *ccdc57*, as the injected groups showed significantly higher expression of *ccdc57* than the uninjected groups by qPCR (Fig. 6B). The angle between the straight line along the yolk sac extension and the line joining the end of yolk sac extension to the tip of the tail was measured to evaluate the curvature degree of the body axis during the embryonic stage. When the spine was curved ventrally, the angle was greater than 180°; otherwise, it was less than 180° (Fig. S5A). The injected groups had significantly smaller degrees than the uninjected groups (Fig. S5B).

CSF flow can regulate urotensin neuropeptide expression by transporting adrenergic signals to neurons along the spinal cord to activate urotensin signaling, contributing to straightening of the body axis (Zhang et al., 2018). To verify this theory, epinephrine treatment was conducted to restore urotensin signaling. Excitingly, epinephrine treatment resulted in dorsal curvature in both WT and *ccdc57* mutant embryos, the same effect as *ccdc57* mRNA injection (Fig. 6C). The angles of each group were measured with ImageJ and arranged into graphics. The angles of WT, epinephrine-treated WT, and epinephrine-treated MZ*ccdc57* mutants were all basically less than 180°, while the angles of MZ*ccdc57* mutants without epinephrine treatment were mostly greater than 180°. Some embryos treated with epinephrine even showed smaller degrees than the WT zebrafish as a result of their dorsal curvature (Fig. S5C). Furthermore, epinephrine treatment significantly induced *urp2* and *uts2r* expression in MZ*ccdc57* mutant embryos (Fig. 6D). Urotensin signaling-related genes, including *urp1*, *urp2*, *uts2r*, and *uts2ra*, which were down-regulated due to *ccdc57* depletion, were dramatically upregulated in *ccdc57* mutant embryos, corresponding to the effect of *ccdc57* overexpression by mRNA injection (Fig. 6E). In addition to the same dorsal curvature effect, both *ccdc57* overexpression and epinephrine treatment resulted in pericardial edema in zebrafish embryos (Fig. S6A and S6B). These results strongly suggested that Ccdc57 regulated the body axis through epinephrine-urotensin signaling in zebrafish.

Discussion

CCDC57 belongs to the family of coiled-coil domain-containing proteins, and other members in this family are associated with cilia development (Panizzi et al., 2012; Horani et al., 2013; Hjeij et al., 2014; Sui et al., 2016; Benjamin et al., 2020; Chen et al., 2021). CCDC57 has been demonstrated to be a pleiotropic regulator of centriole duplication, ciliogenesis, and microtubule stabilization in mammalian cells (Gurkaslar et al., 2020). In this study, we established two *ccdc57* knockout zebrafish strains with frameshift mutations, and both strains displayed the same scoliosis phenotype. The MZ*ccdc57* mutants displayed ventral curvature at the embryonic stage, and this phenotype could be rescued with *ccdc57* mRNA injection. These results strongly demonstrate that *ccdc57* is required for straightening the body axis in zebrafish.

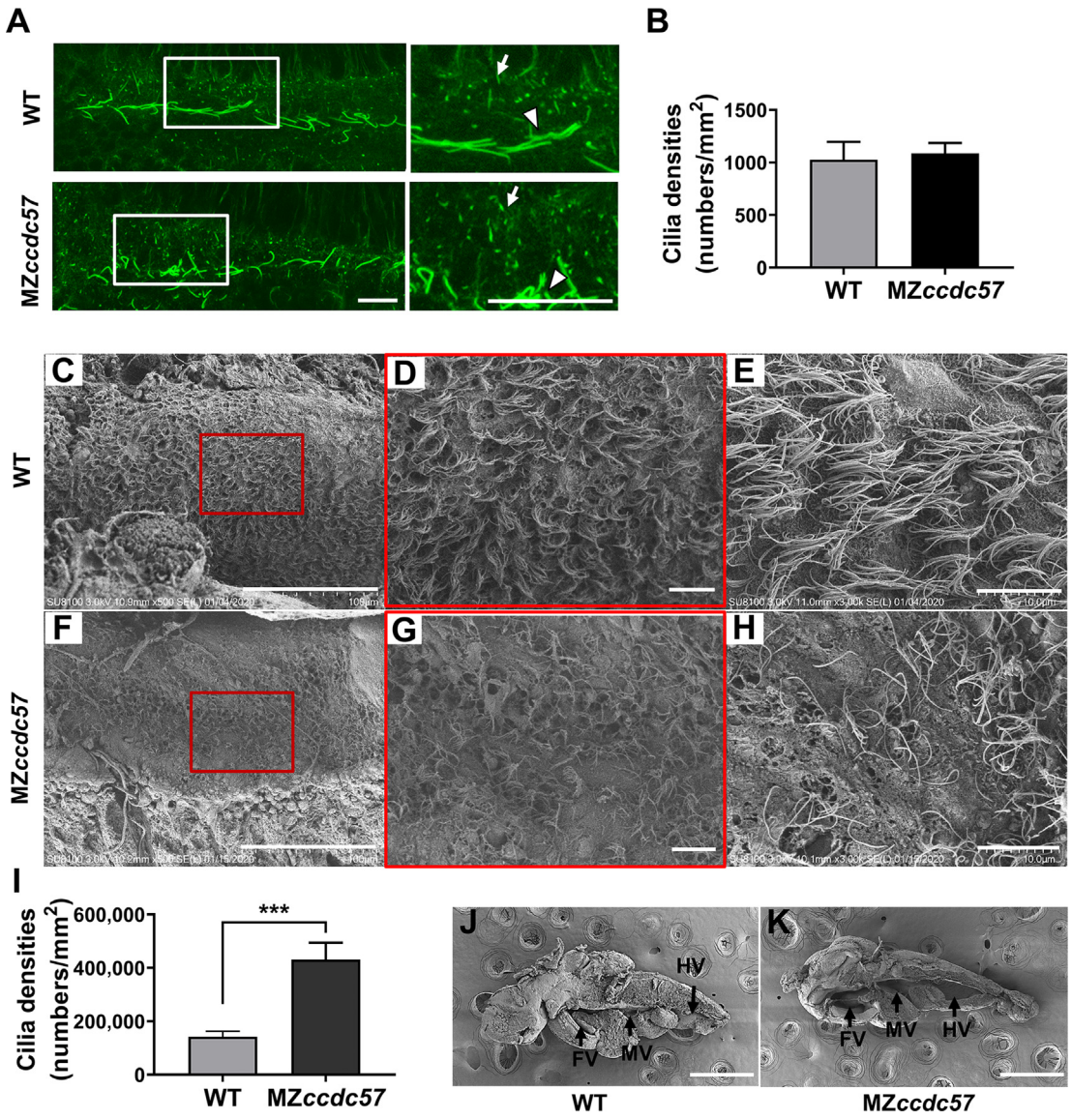

Fig. 4. Examination of cilia in the BV of embryos and adult zebrafish. **A**: Observations of cilia in the BV of WT and MZ*ccdc57* mutant embryos by immunofluorescence analysis. The white boxes indicate the magnified region. The white arrows indicate the cilia in the BV (short). The white arrowheads indicate the cilia in the spinal cord (long). **B**: Analysis of ciliary densities in the BV of WT and MZ*ccdc57* mutant embryos at 48 hpf. **C**–**H**: Observation of cilia in the BV of adult WT and MZ*ccdc57* mutant zebrafish by scanning electron microscopy. The red boxes indicate the magnified region. **I**: Analysis of cilia densities in adult BV reveals significant differences between WT and mutant zebrafish. **J** and **K**: Observation of BV by scanning electron microscopy revealed severe hydrocephalus in *ccdc57* mutant zebrafish. Data were presented as mean ± SD. Statistical analysis was performed by Student's *t*-test. ***, $P < 0.001$. Scale bars, 10 μm (**A**, **D**, **E**, **G**, **H**); 100 μm (**C** and **F**); 1 mm (**J** and **K**). BV, brain ventricle; FV, forebrain ventricle; MV, midbrain ventricle; HV, hindbrain ventricle.

In zebrafish, cilia are well known to exist in the olfactory placode, eye, otic vesicle, BV, pronephros, and spinal canal. Mutants with cilia defects are usually associated with left-right asymmetry defects and kidney cysts (Malicki et al., 2011). Interestingly, the distribution of *ccdc57* mRNA was ubiquitous before the 6-somite stage and then was restricted to specific tissues, such as the BV, otic vesicles, and inner nuclear layer, but not the pronephros and spinal canal. By observation of cilia labeled with fluorescence, we found that the cilia in the BV and otic vesicles were much shorter than the cilia in the pronephros and spinal canal at the embryonic stage. Ccdc57 is likely to play special roles in the shorter cilia of zebrafish during the embryonic stage.

Dysfunction of cilia has been implicated in idiopathic scoliosis (Grimes et al., 2016). Thus, ciliogenesis and ciliary function in BV were examined in our study. Although the *ccdc57* mutant adults displayed severe ciliary abnormalities, we thought that ciliogenesis in BV was not affected at the embryonic stage, as the cilia density and morphology were not changed in *ccdc57* mutant embryos at 48 hpf, when the phenotype of body curvature and compromised CSF flow had occurred. Combined with the fact that *ccdc57* mutant adults also developed hydrocephalus, the adult cilia abnormality was thought to be degenerative results caused by hydrocephalus. Both hydrocephalus and scoliosis are typical phenotypes associated with a loss of EC cilia function (Lee, 2013; Olstad et al., 2019). Since *ccdc57* is not required for ciliogenesis, it is tempting to speculate that *ccdc57* deficiency is associated with ciliary motility defects. This hypothesis was confirmed preliminarily by the compromised CSF flow in *ccdc57* mutant embryos.

Ciliary motility is generated by the outer and inner dynein arms, which control the cilia beat frequency and waveform, respectively

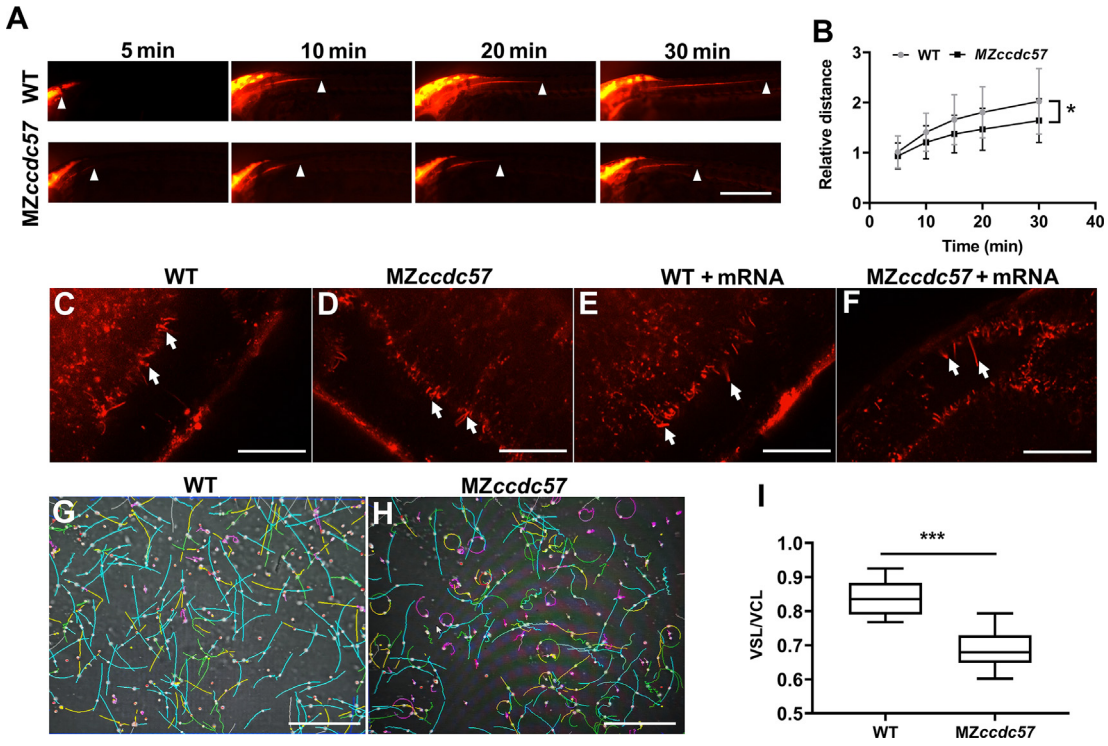

Fig. 5. Ccdc57 deficiency results in compromised CSF flow and an abnormal ciliary beat pattern. **A**: The moving paths of Texas Red-dextran in the spinal canal of WT and MZ*ccdc57* mutant embryos at 72 hpf. **B**: Statistical analysis of the distance traveled by fluorescent beads in WT and MZ*ccdc57* mutant embryos at different time points after injection ($n = 12$). **C**–**F**: Cilia beat pattern in the BV of WT, MZ*ccdc57* mutant, *ccdc57* mRNA-injected, WT, and MZ*ccdc57* mutant embryos detected by confocal microscopy. **G** and **H**: Observation of the swimming paths of WT and MZ*ccdc57* mutant sperms by CASA. **I**: Analyzing the curved degrees of sperm swimming paths based on the ratios of VSL and VCL. Data were presented as mean ± SD. Statistical analysis was performed by Student's *t*-test. *, $P < 0.05$; ***, $P < 0.001$. Scale bars, 100 μm (**A**); 5 μm (**C**–**F**); 50 μm (**G** and **H**). BV, brain ventricle; hpf, hours post fertilization; CASA, computer-assisted sperm analysis; VSL, straight-line velocity; VCL, curvilinear velocity.

(Walczak and Nelson, 1994; Oda et al., 2014; King, 2016). Mutations in genes encoding proteins of the ODAs or in the ODA docking complex system (ODA-DC), including DNAH5, DNAH11, CCDC114, DNAL1, DNAI1, DNAI2, and ARMC4, generally cause outer dynein arm deficiency (Pennarun et al., 1999; Bartoloni et al., 2002; Olbrich et al., 2002; Loges et al., 2008; Mazor et al., 2011; Hjeij et al., 2013; Knowles et al., 2013a). Mutations in genes encoding cytoplasmic proteins, such as SPAG1, DNAAF1, DNAAF2, DNAAF3, HEATR2, DYX1C1, ZMYND10, LRRC6, C21orf59, and CCDC103, cause combined outer and inner dynein arm deficiency (Omran et al., 2008; Loges et al., 2009; Horani et al., 2012; Kott et al., 2012; Mitchison et al., 2012; Panizzi et al., 2012; Austin-Tse et al., 2013; Knowles et al., 2013b; Tarkar et al., 2013; Zariwala et al., 2013). Both CCDC39 and CCDC40 localize to motile cilia, and their mutations result in an isolated inner dynein arm absence (Becker-Heck et al., 2011; Merveille et al., 2011). These outer and inner dynein arm defects result in compromised ciliary beating and PCD.

In this study, the cilia motility and axoneme ultrastructure of both BV cilia and sperm flagellum were examined. The beat frequency of MCB in BV was increased, but the sperm flagellum beat frequency was not affected in *ccdc57* mutant zebrafish. However, the beat pattern of both BV cilia and sperm flagellum was changed due to Ccdc57 deficiency. The swimming path of most mutant sperm was changed into a helicoid or circle instead of a smooth curve approaching a straight line. The abnormal swimming path indicated an asymmetrical beat amplitude in the flagellum/cilia. Furthermore, the rhythmic beating of MCB in the *ccdc57* mutant was disrupted, and it is easy to speculate that the abnormal beat pattern of each cilium disrupts the coordinated beating of MCB. These results are similar to those of a previous study suggesting that knockdown of *cyb5d1* in zebrafish impaired coordinated ciliary beating, with an increased beat frequency, and *cyb5d1* mutant Chlamydomonas exhibited short and kinked tracks (Zhao et al., 2021). We think that the increased beat frequency of MCB cilia in the *ccdc57* mutant may be a result of an uncoordinated beat pattern. Our results suggest that *ccdc57* is essential for maintaining the normal ciliary beating pattern and coordinated beating of MCB in zebrafish.

To determine how Ccdc57 regulates ciliary beating, the ultrastructure of the axoneme was investigated by transmission electron microscopy (TEM). Unfortunately, TEM observation of the BV cilia failed, and the ultrastructure of the flagellar axoneme in *ccdc57* mutant sperm appeared normal. It is proposed that changes in the N-DRC are subtle and not detectable using standard TEM (Horani et al., 2013). Thus, the ultrastructural defects in *ccdc57* mutants might be missed due to the detection limits of standard TEM.

The epinephrine signal transported by CSF flow is important to straighten the body axis in zebrafish. Epinephrine signals are transported to nerve cells around the spinal canal and induce the expression of urotensins, which then bind to their receptors, expressed on slow-twitch muscle cells, to promote contraction supporting body axis extension (Zhang et al., 2018). In this study, urotensin signals were significantly downregulated in *ccdc57* mutant embryos that finally developed ventral curvature. While treated with epinephrine, the curved body axis of *ccdc57* mutants was reversed, even into a dorsal curvature. With its one-directional flow, the speed of CSF flow reflects the total CSF production and the amounts of materials transported. The disrupted cilia beating in *ccdc57* mutants resulted in compromised CSF flow and less epinephrine delivered. Thus, the *ccdc57* mutants finally developed ventral curvature accompanied by downregulated urotensin signaling. However, when treated with an overdose of epinephrine, the epinephrine signal was increased significantly through permeation, and the treated embryos

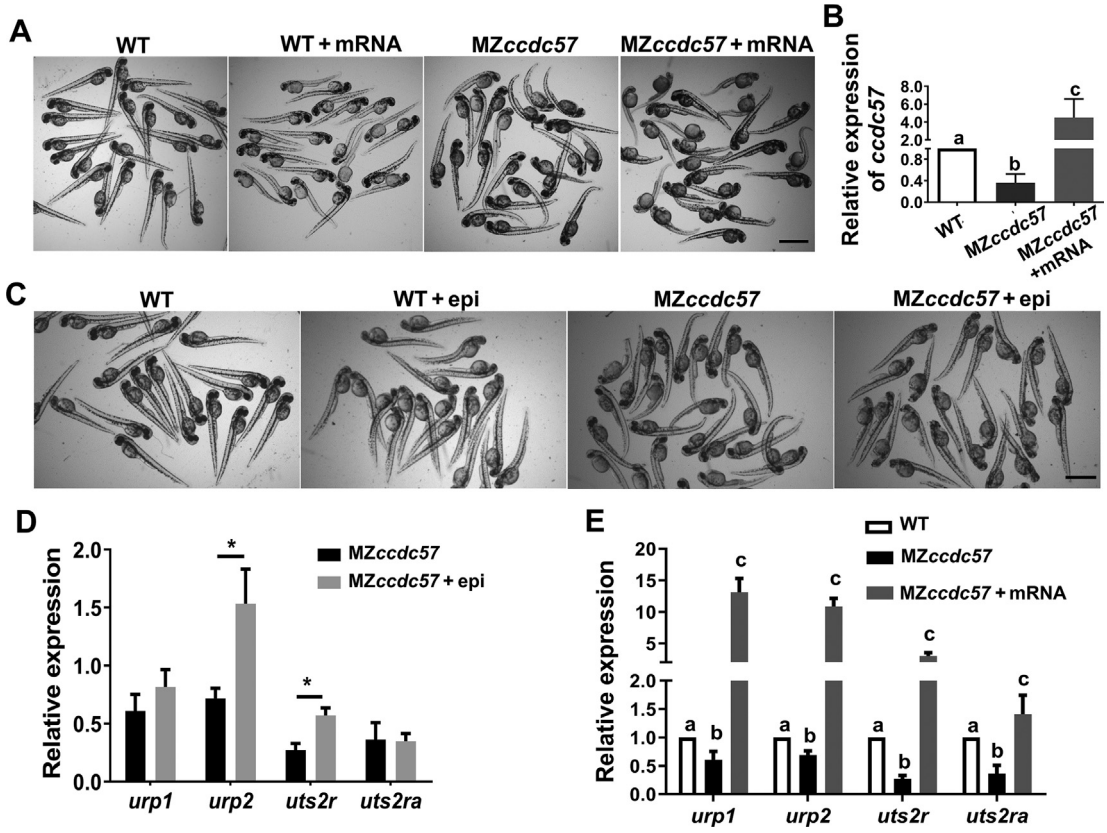

Fig. 6. Rescue experiment by *ccdc57* mRNA injection and epinephrine treatment. **A**: External phenotypes of WT and MZ*ccdc57* mutant embryos and WT and MZ*ccdc57* mutant embryos with *ccdc57* mRNA injection. **B**: Examination of *ccdc57* mRNA levels by qPCR in WT and MZ*ccdc57* mutant embryos and MZ*ccdc57* mutant embryos with *ccdc57* mRNA injection. **C**: External phenotypes of WT and MZ*ccdc57* mutant embryos and WT and MZ*ccdc57* mutant embryos treated with epinephrine. **D**: Relative expression of urotensins and their receptors in MZ*ccdc57* mutant embryos and mutants treated with epinephrine. **E**: Relative expression of urotensins and their receptors in WT, MZ*ccdc57* mutant embryos and MZ*ccdc57* mutant embryos injected with *ccdc57* mRNA. Data were presented as mean ± SD. Statistical analysis performed by one-way ANOVA. Results marked with different letters (a, b, or c) are significantly different ($P < 0.05$). *, $P < 0.05$. Scale bar, 1 mm (**A** and **C**).

could even develop dorsal curvature. Interestingly, overexpression of *ccdc57* could also reverse the body axis of embryos dorsally into the curly phenotype. Observations of ciliary beating revealed coordinated ciliary beating of MCB in *ccdc57*-overexpressing embryos. Thus, it was speculated that the coordination of MCB in WT zebrafish was not saturated and that *ccdc57* overexpression could induce enhanced CSF flow and transport more epinephrine signals. This speculation was confirmed by upregulated urotensin signaling with increased expression of urotensins and their receptors. In addition, both epinephrine treatment and *ccdc57* overexpression led to dorsal curvature effects, as well as edema, in the cardiac cavity. These results strongly demonstrate that *ccdc57* regulates the body axis through epinephrine and urotensin signaling.

In this study, we revealed that dysfunction of *ccdc57* could disrupt the coordinated beating of MCB in BV by changing the cilia beat pattern, resulting in scoliosis in zebrafish. However, the mechanism by which Ccdc57 regulates the cilia beat pattern remains unclear. The precise ultrastructure of the axoneme and the location of the Ccdc57 protein in the axoneme need to be investigated further.

Materials and methods

Zebrafish maintenance

All zebrafish (AB strain) were maintained on a 14-h light and 10-h dark cycle at 28.5°C in a circulated water system and fed newly hatched brine shrimp. All fish experiments were conducted in accordance with the Guiding Principles for the Care and Use of Laboratory Animals and were approved by the Animal Care Committee of Hunan Normal University (Permit Number: 4236). The fish were deeply anesthetized with 0.016% tricaine (Sigma–Aldrich, St. Louis, MO, USA) before dissection.

Generation of the *ccdc57* knockout line

ccdc57 was knocked out via the CRISPR/Cas9 strategy. The target in the first exon of *ccdc57* was: GGAGGAAAGGGACAAAGAGC. The gRNA was transcribed with a TranscriptAid T7 High Yield Transcription Kit (K0441, Thermo Scientific Fermentas, Waltham, MA, USA). Cas9 mRNA was synthesized using the T3 mMESSAGE mMACHINE Kit (AM1348, Ambion, Austin, TX, USA). A mixture with gRNA and Cas9 mRNA at 50 ng/μL and 100 ng/μL, respectively, was injected into one- or two-cell stage embryos. The target region was amplified using the primers listed in Table S1. The genotype of the mutant zebrafish was identified through Sanger sequencing in the F1 population. The homozygotes were obtained by crossing F1 mutants with the same genotype. Groups with different genotypes in the F2 population were identified using DNA PAGE gel electrophoresis.

Calcein staining

Immersion solutions (0.2%) were prepared by dissolving 2 g of calcein powder (Sigma Chemical, St. Louis, MO) in 1 L of deionized water with an appropriate amount of NaOH (0.5 N) added to restore the pH to neutral. Zebrafish embryos were immersed in the solution in Petri dishes for 10 min and then rinsed twice in fresh water for 5 min

each to eliminate nonspecific binding. The embryos were then placed in 1% methylcellulose in confocal dishes, and observations were carried out using a Leica M205 FCA microscope.

Micro-CT

Adult zebrafish were fixed in 4% paraformaldehyde overnight at 4°C. Fixed specimens were mounted in 1% low-melt agarose (Sigma) in a plastic vial. Samples were scanned for 1 h using a SkyScan1172 high resolution Micro-CT scanner (Bruker Micro-CT, Belgium) with X-ray power at 45 kVp and 218 mA. All three-dimensional micro-CT datasets were reconstructed with 18 μm isotropic resolution. The images were then analyzed using Amira software (TGS Inc., Berlin, Germany).

ccdc57 mRNA injection

The *ccdc57* cDNA sequence was amplified from the embryo-stage cDNA and cloned into the pCSII vector with the primers listed in Table S2. The constructed plasmid was linearized and transcribed using the Sp6 mMessage mMachine kit (Invitrogen, USA). Purified *ccdc57* mRNA was collected from the reaction system after LiCl precipitation and injected into one-cell-stage embryos at a concentration of 20 ng/μL.

Whole-mount in situ hybridization

Fragments of *ccdc57* cDNA from 2681 to 3127 base pairs were amplified with the primers listed in Table S3. The *ccdc57* fragment was cloned into the pGEM-T vector, linearized and then transcribed into antisense probes labeled with digoxigenin-UTP. The procedure was carried out as described previously (Thisse and Thisse, 2008).

Fluorescent dye injection

Embryos were anesthetized with 0.2 mg/mL tricaine at 3 dpf and then incubated with 20 mM 2,3-butanedione monoxime (BDM, Sigma) for 5 min to stop the heartbeat. Next, they were placed in the groove of a 1% agarose plate in a drop of egg water as previously described (Lowery and Sive, 2005). The anterior ventricle was microinjected with 2 nL–10 nL dextran conjugated to rhodamine (5% in 0.2 mol/L KCl, Sigma). The fluorescent molecules then diffused through the brain cavities, and micrographs were taken at 5 min, 10 min, 15 min, 20 min, and 30 min with a Leica M205 FCA microscope after injection. The distance that the dye traveled was measured using ImageJ software.

Immunofluorescence of whole embryos

The cilia were visualized by immunofluorescence with a mouse anti-acetylated α-tubulin antibody (T6793; Sigma) and a goat anti-mouse secondary antibody, performed as described previously (Jaffe et al., 2010). An HA-tagged version of *ccdc57* mRNA was injected into the embryos to investigate the localization of Ccdc57, and immunofluorescence was performed with a rabbit anti-HA antibody (3724T, CST) and a goat anti-rabbit secondary antibody. Confocal images of the cilia in the embryonic brains were taken with an FV1200 microscope (Olympus, Japan) under 100× objective lenses, with the head of the embryo squashed onto slides. The lengths of the brain cilia were measured by using ImageJ software. Statistical analysis was performed using Student's *t*-test.

Scanning electron microscopy (SEM)

Adult zebrafish were decapitated, and the brains were removed from the skull and surrounding tissue. Isolated whole brains were immediately fixed by immersion in 2.5% glutaraldehyde for 1 h and then sliced on the sagittal plane along the midline and fixed in 2.5% glutaraldehyde overnight at 4°C. The samples were then rinsed in 0.1 M sodium cacodylate buffer with 0.2 M sucrose (pH 7.3) and gradually dehydrated in an ethanol gradient. The samples were mounted on aluminum stubs, vacuum dried, coated with gold, and then imaged on a JSM-6360 LV SEM (Japan).

Transmission electron microscopy (TEM)

Zebrafish testes were collected and fixed in 2.5% glutaraldehyde, postfixed with 1% OsO4 in the presence of potassium ferricyanide, dehydrated through an ethanol series, transitioned to propylene oxide and embedded in epoxide resin. Ultrathin sections were picked up on 300-mesh copper grids, poststained with 6.25% uranyl acetate in 50% methanol, and examined with an HT7800 transmission electron microscope (Japan).

Ciliary beating observation

The cilia axoneme of zebrafish was labeled with Red Fluorescence Protein by injecting *arl13b-RFP* mRNA into one-cell stage embryos at a concentration of 150 ng/μL. Then, the injected embryos at 24 hpf were observed, and ciliary motility was recorded using a dragonfly microscope (Dragonfly, Andor Technology, UK) at a speed of 100 frame/s.

Computer-assisted sperm analysis (CASA)

The semen of WT and *ccdc57* mutant males was collected and stored in Hanks' solution. Then, the sperm were activated by adding fresh water, and the sperm motility parameters were calculated through CASA. The value of each parameter was determined using the Sperm Quality Analyzer according to the manufacturer's instructions (CEROS II, Australia). Statistical analysis was performed using Student's *t*-test.

Epinephrine treatment

WT and mutant embryos from the bud stage (10 hpf) were treated with epinephrine (Sigma E4642) at a final concentration of 10 mg/mL in the egg water. The epinephrine was refreshed every 4 h during the daytime. After treatment, images were captured using an M165FC microscope equipped with a Leica DFC450C camera.

RT-PCR and qPCR

Total RNA was purified from embryos using TRIzol reagent (Invitrogen, Carlsbad, CA, USA) according to standard protocols. The cDNAs were synthesized using the Reverse Aid First-Strand cDNA Synthesis Kit (K1622, Thermo Scientific, Waltman, MA, USA) according to the manufacturer's instructions. PCR primers spanning the introns were designed based on the National Center for Biotechnology Information (NCBI) database, as listed in Table S4. The qPCR was performed using PowerUp SYBR Green Master Mix on an ABI QuantStudio™ 5 Real-Time PCR System (Life Technologies, USA).

CRediT authorship contribution statement

Lu Li: Conceptualization, Data curation, Methodology, Formal analysis, Investigation, Validation. **Juan Li**: Investigation, Methodology, Resources. **Yuan Ou** and **Jiaxin Wu**: Methodology, Resources, Data curation. **Huilin Li** and **Xin Wang**: Investigation, Resources. **Liying Tang**: Investigation. **Xiangyan Dai**, **Conghui Yang**, **Zehong Wei**: Investigation, Methodology. **Zhan Yin**: Formal analysis. **Yuqin Shu**: Conceptualization, Resources, Supervision, Writing - Review & Editing, Project administration, Funding acquisition.

Conflict of interest

The authors declare that they have no conflict of interest.

Acknowledgments

We thank Professor Zhu from Xidian University for conducting the micro-CT scanning and analysis, professors Jin and Li from East China Normal University for giving the *arl13b-RFP* mRNA as a gift. This work was supported by the National Key Research and Development Program, China (2018YFD0900406), the National Natural Science Foundation, China (31802291), and the Natural Science Foundation of Hunan Province (2021JJ40342).

Supplementary data

Supplementary data to this article can be found online at https://doi.org/10.1016/j.jgg.2022.12.007.

References

Aissani, B., Zhang, K., Wiener, H., 2015. Evaluation of GWAS candidate susceptibility loci for uterine leiomyoma in the multi-ethnic NIEHS uterine fibroid study. Front. Genet. 6, 241.

Alleyne, A.T., Bideau, V.S., 2019. Haplotypes of *CYP1B1* and *CCDC57* genes in an Afro-Caribbean female population with uterine leiomyoma. Mol. Biol. Rep. 46, 3299–3306.

Austin-Tse, C., Halbritter, J., Zariwala, M.A., Gilberti, R.M., Gee, H.Y., Hellman, N., Pathak, N., Liu, Y., Panizzi, J.R., Patel-King, R.S., et al., 2013. Zebrafish ciliopathy screen plus human mutational analysis identifies *C21orf59* and *CCDC65* defects as causing primary ciliary dyskinesia. Am. J. Hum. Genet. 93, 672–686.

Bartoloni, L., Blouin, J.L., Pan, Y., Gehrig, C., Maiti, A.K., Scamuffa, N., Rossier, C., Jorissen, M., Armengot, M., Meeks, M., et al., 2002. Mutations in the *DNAH11* (axonemal heavy chain dynein type 11) gene cause one form of situs inversus totalis and most likely primary ciliary dyskinesia. Proc. Natl. Acad. Sci. U. S. A. 99, 10282–10286.

Bazan, R., Schrofel, A., Joachimiak, E., Poprzeczko, M., Pigino, G., Wloga, D., 2021. Ccdc113/Ccdc96 complex, a novel regulator of ciliary beating that connects radial spoke 3 to dynein g and the nexin link. PLoS Genet. 17, e1009388.

Becker-Heck, A., Zohn, I.E., Okabe, N., Pollock, A., Lenhart, K.B., Sullivan-Brown, J., McSheene, J., Loges, N.T., Olbrich, H., Haeffner, K., et al., 2011. The coiled-coil domain containing protein CCDC40 is essential for motile cilia function and left-right axis formation. Nat. Genet. 43, 79–84.

Benjamin, A.T., Ganesh, R., Chinnappa, J., Kinimi, I., Lucas, J., 2020. Primary ciliary dyskinesia due to *DRC1/CCDC164* gene mutation. Lung India 37, 179–180.

Blanchon, S., Legendre, M., Copin, B., Duquesnoy, P., Montantin, G., Kott, E., Dastot, F., Jeanson, L., Cachanado, M., Rousseau, A., et al., 2012. Delineation of *CCDC39/CCDC40* mutation spectrum and associated phenotypes in primary ciliary dyskinesia. J. Med. Genet. 49, 410–416.

Bohlouli, M., Halli, K., Yin, T., Gengler, N., Konig, S., 2022. Genome-wide associations for heat stress response suggest potential candidate genes underlying milk fatty acid composition in dairy cattle. J. Dairy Sci. 105, 3323–3340.

Bouwman, A.C., Visker, M.H., van Arendonk, J.M., Bovenhuis, H., 2014. Fine mapping of a quantitative trait locus for bovine milk fat composition on *Bos taurus* autosome 19. J. Dairy Sci. 97, 1139–1149.

Burkhard, P., Stetefeld, J., Strelkov, S.V., 2001. Coiled coils: a highly versatile protein folding motif. Trends Cell Biol. 11, 82–88.

Cannarella, R., Maniscalchi, E.T., Condorelli, R.A., Scalia, M., Guerri, G., La Vignera, S., Bertelli, M., Calogero, A.E., 2020. Ultrastructural sperm flagellum defects in a patient with *CCDC39* compound heterozygous mutations and primary ciliary dyskinesia/*situs viscerum inversus*. Front. Genet. 11, 974.

Chen, D., Liang, Y., Li, J., Zhang, X., Zheng, R., Wang, X., Zhang, H., Shen, Y., 2021. A novel *CCDC39* mutation causes multiple morphological abnormalities of the flagella in a primary ciliary dyskinesia patient. Reprod. Biomed. Online 43, 920–930.

Chen, X., Deng, S., Xia, H., Yuan, L., Xu, H., Tang, S., Deng, H., 2020. Identification of a *CCDC114* variant in a Han-Chinese patient with situs inversus. Exp. Ther. Med. 20, 3336–3342.

Deng, S., Wu, S., Xia, H., Xiong, W., Deng, X., Liao, J., Deng, H., Yuan, L., 2020. Identification of a frame shift mutation in the *CCDC151* gene in a Han-Chinese family with Kartagener syndrome. Biosci. Rep. 40, BSR20192510.

Escudier, E., Duquesnoy, P., Papon, J.F., Amselem, S., 2009. Ciliary defects and genetics of primary ciliary dyskinesia. Paediatr. Respir. Rev. 10, 51–54.

Firat-Karalar, E.N., Sante, J., Elliott, S., Stearns, T., 2014. Proteomic analysis of mammalian sperm cells identifies new components of the centrosome. J. Cell Sci. 127, 4128–4133.

Grimes, D.T., Boswell, C.W., Morante, N.F., Henkelman, R.M., Burdine, R.D., Ciruna, B., 2016. Zebrafish models of idiopathic scoliosis link cerebrospinal fluid flow defects to spine curvature. Science 352, 1341–1344.

Gurkaslar, H.K., Culfa, E., Arslanhan, M.D., Lince-Faria, M., Firat-Karalar, E.N., 2020. CCDC57 cooperates with microtubules and microcephaly protein CEP63 and regulates centriole duplication and mitotic progression. Cell Rep. 31, 107630.

Harbury, P.B., Plecs, J.J., Tidor, B., Alber, T., Kim, P.S., 1998. High-resolution protein design with backbone freedom. Science 282, 1462–1467.

Hayes, M., Gao, X., Yu, L.X., Paria, N., Henkelman, R.M., Wise, C.A., Ciruna, B., 2014. *ptk7* mutant zebrafish models of congenital and idiopathic scoliosis implicate dysregulated Wnt signalling in disease. Nat. Commun. 5, 4777.

Hjeij, R., Lindstrand, A., Francis, R., Zariwala, M.A., Liu, X., Li, Y., Damerla, R., Dougherty, G.W., Abouhamed, M., Olbrich, H., et al., 2013. *ARMC4* mutations cause primary ciliary dyskinesia with randomization of left/right body asymmetry. Am. J. Hum. Genet. 93, 357–367.

Hjeij, R., Onoufriadis, A., Watson, C.M., Slagle, C.E., Klena, N.T., Dougherty, G.W., Kurkowiak, M., Loges, N.T., Diggle, C.P., Morante, N.F., et al., 2014. *CCDC151* mutations cause primary ciliary dyskinesia by disruption of the outer dynein arm docking complex formation. Am. J. Hum. Genet. 95, 257–274.

Horani, A., Brody, S.L., Ferkol, T.W., Shoseyov, D., Wasserman, M.G., Ta-shma, A., Wilson, K.S., Bayly, P.V., Amirav, I., Cohen-Cymberknoh, M., et al., 2013. *CCDC65* mutation causes primary ciliary dyskinesia with normal ultrastructure and hyperkinetic cilia. PLoS ONE 8, e72299.

Horani, A., Druley, T.E., Zariwala, M.A., Patel, A.C., Levinson, B.T., Van Arendonk, L.G., Thornton, K.C., Giacalone, J.C., Albee, A.J., Wilson, K.S., et al., 2012. Whole-exome capture and sequencing identifies *HEATR2* mutation as a cause of primary ciliary dyskinesia. Am. J. Hum. Genet. 91, 685–693.

Huang, N., Xia, Y., Zhang, D., Wang, S., Bao, Y., He, R., Teng, J., Chen, J., 2017. Hierarchical assembly of centriole subdistal appendages via centrosome binding proteins CCDC120 and CCDC68. Nat. Commun. 8, 15057.

Ishikawa, T., 2017. Axoneme structure from motile cilia. Cold Spring Harbor Perspect. Biol. 9, a028076.

Jaffe, K.M., Thiberge, SY., Bisher, ME., Burdine, R.D., 2010. Imaging cilia in zebrafish. Methods Cell Biol. 97, 415–435.

Jerber, J., Baas, D., Soulavie, F., Chhin, B., Cortier, E., Vesque, C., Thomas, J., Durand, B., 2014. The coiled-coil domain containing protein CCDC151 is required for the function of IFT-dependent motile cilia in animals. Hum. Mol. Genet. 23, 563–577.

Joo, K., Kim, C.G., Lee, M.S., Moon, H.Y., Lee, S.H., Kim, M.J., Kweon, H.S., Park, W.Y., Kim, C.H., Gleeson, J.G., et al., 2013. CCDC41 is required for ciliary vesicle docking to the mother centriole. Proc. Natl. Acad. Sci. U. S. A. 110, 5987–5992.

King, S.M., 2016. Axonemal dynein arms. Cold Spring Harbor Perspect. Biol. 8, a028100.

Knowles, M.R., Leigh, M.W., Ostrowski, L.E., Huang, L., Carson, J.L., Hazucha, M.J., Yin, W., Berg, J.S., Davis, S.D., Dell, S.D., et al., 2013a. Exome sequencing identifies mutations in *CCDC114* as a cause of primary ciliary dyskinesia. Am. J. Hum. Genet. 92, 99–106.

Knowles, M.R., Ostrowski, L.E., Loges, N.T., Hurd, T., Leigh, M.W., Huang, L., Wolf, W.E., Carson, J.L., Hazucha, M.J., Yin, W., et al., 2013b. Mutations in *SPAG1* cause primary ciliary dyskinesia associated with defective outer and inner dynein arms. Am. J. Hum. Genet. 93, 711–720.

Kott, E., Duquesnoy, P., Copin, B., Legendre, M., Dastot-Le Moal, F., Montantin, G., Jeanson, L., Tamalet, A., Papon, J.F., Siffroi, J.P., et al., 2012. Loss-of-function mutations in *LRRC6*, a gene essential for proper axonemal assembly of inner and outer dynein arms, cause primary ciliary dyskinesia. Am. J. Hum. Genet. 91, 958–964.

Lee, L., 2013. Riding the wave of ependymal cilia: genetic susceptibility to hydrocephalus in primary ciliary dyskinesia. J. Neurosci. Res. 91, 1117–1132.

Li, P., He, Y., Cai, G., Xiao, F., Yang, J., Li, Q., Chen, X., 2019. *CCDC114* is mutated in patient with a complex phenotype combining primary ciliary dyskinesia, sensorineural deafness, and renal disease. J. Hum. Genet. 64, 39–48.

Loges, N.T., Olbrich, H., Becker-Heck, A., Haffner, K., Heer, A., Reinhard, C., Schmidts, M., Kispert, A., Zariwala, M.A., Leigh, M.W., et al., 2009. Deletions and point mutations of *LRRC50* cause primary ciliary dyskinesia due to dynein arm defects. Am. J. Hum. Genet. 85, 883–889.

Loges, N.T., Olbrich, H., Fenske, L., Mussaffi, H., Horvath, J., Fliegauf, M., Kuhl, H., Baktai, G., Peterffy, E., Chodhari, R., et al., 2008. *DNAI2* mutations cause primary ciliary dyskinesia with defects in the outer dynein arm. Am. J. Hum. Genet. 83, 547–558.

Lokaj, M., Kosling, S.K., Koerner, C., Lange, S.M., van Beersum, S.E., van Reeuwijk, J., Roepman, R., Horn, N., Ueffing, M., Boldt, K., et al., 2015. The

interaction of CCDC104/BARTL1 with Arl3 and implications for ciliary function. Structure 23, 2122–2132.
Lowery, L.A., Sive, H., 2005. Initial formation of zebrafish brain ventricles occurs independently of circulation and requires the *nagie oko* and s*nakehead/atp1a1a.1* gene products. Development 132, 2057–2067.
Lupas, A., 1996. Coiled coils: new structures and new functions. Trends Biochem. Sci. 21, 375–382.
Lupas, A.N., Bassler, J., Dunin-Horkawicz, S., 2017. The structure and topology of alpha-helical coiled coils. Subcell. Biochem. 82, 95–129.
Mahjoub, M.R., Xie, Z., Stearns, T., 2010. Cep120 is asymmetrically localized to the daughter centriole and is essential for centriole assembly. J. Cell Biol. 191, 331–346.
Malicki, J., Avanesov, A., Li, J., Yuan, S., Sun, Z., 2011. Analysis of cilia structure and function in zebrafish. Methods Cell Biol. 101, 39–74.
Mazor, M., Alkrinawi, S., Chalifa-Caspi, V., Manor, E., Sheffield, V.C., Aviram, M., Parvari, R., 2011. Primary ciliary dyskinesia caused by homozygous mutation in *DNAL1*, encoding dynein light chain 1. Am. J. Hum. Genet. 88, 599–607.
Merveille, A.C., Davis, E.E., Becker-Heck, A., Legendre, M., Amirav, I., Bataille, G., Belmont, J., Beydon, N., Billen, F., Clement, A., et al., 2011. CCDC39 is required for assembly of inner dynein arms and the dynein regulatory complex and for normal ciliary motility in humans and dogs. Nat. Genet. 43, 72–78.
Mitchison, H.M., Schmidts, M., Loges, N.T., Freshour, J., Dritsoula, A., Hirst, R.A., O'Callaghan, C., Blau, H., Al Dabbagh, M., Olbrich, H., et al., 2012. Mutations in axonemal dynein assembly factor *DNAAF3* cause primary ciliary dyskinesia. Nat. Genet. 44, 381–389.
Ochi, T., Quarantotti, V., Lin, H., Jullien, J., Rosa, E.S.I., Boselli, F., Barnabas, D.D., Johnson, C.M., McLaughlin, S.H., Freund, S.M.V., et al., 2020. CCDC61/VFL3 is a paralog of SAS6 and promotes ciliary functions. Structure 28, 674–689.
Oda, T., Yanagisawa, H., Kamiya, R., Kikkawa, M., 2014. A molecular ruler determines the repeat length in eukaryotic cilia and flagella. Science 346, 857–860.
Olbrich, H., Haffner, K., Kispert, A., Volkel, A., Volz, A., Sasmaz, G., Reinhardt, R., Hennig, S., Lehrach, H., Konietzko, N., et al., 2002. Mutations in *DNAH5* cause primary ciliary dyskinesia and randomization of left-right asymmetry. Nat. Genet. 30, 143–144.
Olstad, E.W., Ringers, C., Hansen, J.N., Wens, A., Brandt, C., Wachten, D., Yaksi, E., Jurisch-Yaksi, N., 2019. Ciliary beating compartmentalizes cerebrospinal fluid flow in the brain and regulates ventricular development. Curr. Biol. 29, 229–241.
Omran, H., Kobayashi, D., Olbrich, H., Tsukahara, T., Loges, N.T., Hagiwara, H., Zhang, Q., Leblond, G., O'Toole, E., Hara, C., et al., 2008. Ktu/PF13 is required for cytoplasmic pre-assembly of axonemal dyneins. Nature 456, 611–616.
Onoufriadis, A., Paff, T., Antony, D., Shoemark, A., Micha, D., Kuyt, B., Schmidts, M., Petridi, S., Dankert-Roelse, J.E., Haarman, E.G., et al., 2013. Splice-site mutations in the axonemal outer dynein arm docking complex gene *CCDC114* cause primary ciliary dyskinesia. Am. J. Hum. Genet. 92, 88–98.
Panizzi, J.R., Becker-Heck, A., Castleman, V.H., Al-Mutairi, D.A., Liu, Y., Loges, N.T., Pathak, N., Austin-Tse, C., Sheridan, E., Schmidts, M., et al., 2012. *CCDC103* mutations cause primary ciliary dyskinesia by disrupting assembly of ciliary dynein arms. Nat. Genet. 44, 714–719.
Pennarun, G., Escudier, E., Chapelin, C., Bridoux, A.M., Cacheux, V., Roger, G., Clement, A., Goossens, M., Amselem, S., Duriez, B., 1999. Loss-of-function mutations in a human gene related to *Chlamydomonas reinhardtii* dynein *IC78* result in primary ciliary dyskinesia. Am. J. Hum. Genet. 65, 1508–1519.
Pizon, V., Gaudin, N., Poteau, M., Cifuentes-Diaz, C., Demdou, R., Heyer, V., Reina San Martin, B., Azimzadeh, J., 2020. hVFL3/CCDC61 is a component of mother centriole subdistal appendages required for centrosome cohesion and positioning. Biol. Cell. 112, 22–37.
Priyanka, P.P., Yenugu, S., 2021. Coiled-coil domain-containing (CCDC) proteins: functional roles in general and male reproductive physiology. Reprod. Sci. 28, 2725–2734.
Rackham, O.J., Madera, M., Armstrong, C.T., Vincent, T.L., Woolfson, D.N., Gough, J., 2010. The evolution and structure prediction of coiled coils across all genomes. J. Mol. Biol. 403, 480–493.
Rose, A., Schraegle, S.J., Stahlberg, E.A., Meier, I., 2005. Coiled-coil protein composition of 22 proteomes–differences and common themes in subcellular infrastructure and traffic control. BMC Evol. Biol. 5, 66.
Silva, E., Betleja, E., John, E., Spear, P., Moresco, J.J., Zhang, S., Yates 3rd, J.R., Mitchell, B.J., Mahjoub, M.R., 2016. Ccdc11 is a novel centriolar satellite protein essential for ciliogenesis and establishment of left-right asymmetry. Mol. Biol. Cell 27, 48–63.
Stetefeld, J., Jenny, M., Schulthess, T., Landwehr, R., Engel, J., Kammerer, R.A., 2000. Crystal structure of a naturally occurring parallel right-handed coiled coil tetramer. Nat. Struct. Biol. 7, 772–776.
Sui, W., Hou, X., Che, W., Ou, M., Sun, G., Huang, S., Liu, F., Chen, P., Wei, X., Dai, Y., 2016. *CCDC40* mutation as a cause of primary ciliary dyskinesia: a case report and review of literature. Clin. Res. J. 10, 614–621.
Tarkar, A., Loges, N.T., Slagle, C.E., Francis, R., Dougherty, G.W., Tamayo, J.V., Shook, B., Cantino, M., Schwartz, D., Jahnke, C., et al., 2013. DYX1C1 is required for axonemal dynein assembly and ciliary motility. Nat. Genet. 45, 995–1003.
Thisse, C., Thisse, B., 2008. High-resolution in situ hybridization to whole-mount zebrafish embryos. Nat. Protoc. 3, 59–69.
Truebestein, L., Leonard, T.A., 2016. Coiled-coils: the long and short of it. Bioessays 38, 903–916.
Walczak, C.E., Nelson, D.L., 1994. Regulation of dynein-driven motility in cilia and flagella. Cell Motil. Cytoskeleton 27, 101–107.
Wu, D.H., Singaraja, R.R., 2013. Loss-of-function mutations in *CCDC114* cause primary ciliary dyskinesia. Clin. Genet. 83, 526–527.
Zariwala, M.A., Gee, H.Y., Kurkowiak, M., Al-Mutairi, D.A., Leigh, M.W., Hurd, T.W., Hjeij, R., Dell, S.D., Chaki, M., Dougherty, G.W., et al., 2013. *ZMYND10* is mutated in primary ciliary dyskinesia and interacts with LRRC6. Am. J. Hum. Genet. 93, 336–345.
Zhang, X., Jia, S., Chen, Z., Chong, Y.L., Xie, H., Feng, D., Wu, X., Song, D.Z., Roy, S., Zhao, C., 2018. Cilia-driven cerebrospinal fluid flow directs expression of urotensin neuropeptides to straighten the vertebrate body axis. Nat. Genet. 50, 1666–1673.
Zhao, L., Xie, H., Kang, Y., Lin, Y., Liu, G., Sakato-Antoku, M., Patel-King, R.S., Wang, B., Wan, C., King, S.M., et al., 2021. Heme-binding protein CYB5D1 is a radial spoke component required for coordinated ciliary beating. Proc. Natl. Acad. Sci. U. S. A. 118, e201568911.